JOURNAL OF CATALYSIS 117, 322–334 (1989)

Paraffin Isomerization and Disproportionation Catalyzed by Pd-Loaded Fluorided Mordenites

JAMES A. MANESS, JR.,[1] AND KERRY M. DOOLEY[2]

Department of Chemical Engineering, Louisiana State University, Baton Rouge, Louisiana 70803

Received June 15, 1988; revised November 8, 1988

Fluorided, Pd-loaded (~1.1 wt% Pd) mordenites, with 8, 12, 28, and 100% replacement of –OH groups, were synthesized from H-mordenite. These materials were characterized by IR, XRD, SEM, the adsorption of N_2 and 2-methylpentane, and their activity for paraffin reactions. Except in the case of 100% nominal fluoridation, the fluorided mordenites retained their crystallinity, displayed enhanced acid strengths and adsorption capacities for paraffinic hydrocarbons, and were catalytically active (at 533–573 K and ~0.1 bar hydrocarbon partial pressure) for the transformation of *n*-butane to isobutane and products of both higher and lower molecular weights. The presence of a small amount of isobutene in the feed greatly accelerated these transformations and increased yields to the pentane isomers. The primary reactions were apparently acid-catalyzed, with the role of Pd confined to activity maintenance. The mildly fluorided zeolites in some cases proved more active overall than the parent zeolites H-mordenite and Pd-mordenite and were especially selective for the formation of the pentane isomers, apparently through a combination of disproportionation reactions and secondary alkylation reactions involving light hydrocarbon primary products.

INTRODUCTION

The incorporation of fluorine in zeolites or silica–aluminas has been practiced to increase their activity for acid-catalyzed reactions such as *n*-butane isomerization, alkylation of alkanes with light olefins, and cumene cracking (*1, 2*). Surface hydroxyls are replaced by F^- ions, which, because of the slightly higher electronegativity of fluorine, may polarize the lattice more than the groups they replace and therefore enhance acid strengths.

Gas-phase fluoridation and ion exchange using aqueous solutions are the two common methods of incorporating F^- in zeolites. Gas-phase fluoridation can affect zeolite crystal structure; treatment with F_2 under ambient conditions substantially dealuminates pentasils, mordenite, erionite, and zeolite Y (*3*). The ion-exchange technique seemingly results in minimal dealumination, according to X-ray results (*4*), although exchange with aqueous HF can sometimes dealuminate the crystals or react the aluminum to AlF_3, depending upon the solution molarity (*5*).

The acid strengths of the acid sites remaining after fluoridation are indicated by the initial enthalpy of NH_3 adsorption. At 416 K these values (in kJ/mol) are as follows: HY, 125 and ZSM-5, 150 (*6*); mordenite, 155 and an ion-exchanged, fluorided mordenite, 200 (*4*). This last value is about 30 kJ/mol higher than that obtained for NH_3 adsorbed on a solid superacid prepared from SbF_5 and silica–alumina (*7*).

The nature of these acid sites depends upon the nature of the fluoride treatment and subsequent calcinations; the chemistry of fluoride incorporation may be quite complex. For mild fluoridations (typically those resulting in $<\sim$10% nominal –OH replacement) the number of low-temperature Brønsted acid sites apparently increases (*5*), while for more severe fluoride

[1] Present address: International Paper Co., P.O. Box 2787, Mobile, AL 36652.

[2] To whom all correspondence should be addressed.

0021-9517/89 $3.00

treatments this number decreases significantly (*4*). The new low-temperature Brønsted sites may result from the association of water with Lewis sites that can be generated by fluoride replacement, for example,

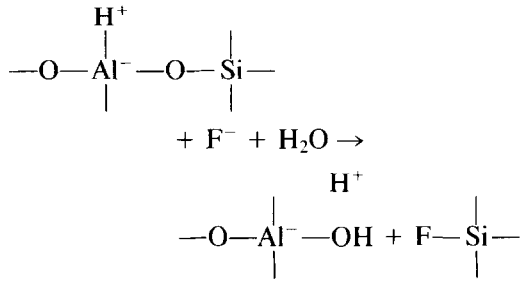

As expected, these Brønsted sites are converted to Lewis sites at temperatures >~550 K. This chemistry is in accord with the fluoridation chemistry of silica–aluminas as eluciated by CP-MAS NMR studies (*8*).

The skeletal isomerization of *n*-butane can be used not only to gauge the acid strengths of fluorided zeolites and amorphous oxides but also to estimate their activity for more complex normal paraffin alkylation reactions; both reaction mechanisms involve secondary carbenium ion intermediates and both include a hydride abstraction (*9, 10*). Trace amounts of olefins often supply an adequate amount of carbocation chain-carriers for these reactions, without causing excessive by-product formation. With strong acid catalysts and in the absence of olefin initiators, the isomerization reaction in solution proceeds through a penta-coordinated carbonium (nonclassical) ion as (*11*)

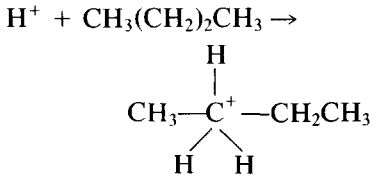

Haag and Dessau (*12*) have postulated that for low hydrocarbon partial pressures and high temperatures the nonclassical ion may be present on solid acids, resulting in protolytic cracking to light hydrocarbons as observed by them and others (*13–15*). In this study high *n*-butane partial pressures and carefully regulated amounts of an olefin intiator were used in an attempt to limit yields to cracking products. Our intent was not to fully characterize the surface chemistry of fluorided mordenites, but rather to examine their advantages and disadvantages as strong acid catalysts.

EXPERIMENTAL

Catalyst Preparation

Commercial mordenite (Linde M-8, SiO_2/Al_2O_3 = 17.0) was dried at 800 K and then added to a dilute solution of NH_4F (Alfa, reagent) in a Teflon beaker. The molarity of the solution was adjusted to vary the percentage replacement of hydroxyl groups; for example, for sample A3 (27.6% nominal replacement of –OH groups) a 0.3 *M* solution was used. After 20 h contact time, the slurry was filtered and evaporated to dryness, and the zeolite was calcined in air at 700 K.

A series of modified mordenites containing about 1 wt% Pd was prepared by ion exchange with a dilute solution of $[Pd(NH_3)_4](OH)_2$, which in turn was prepared by passing a tetraammine chloride solution (from Aldrich $PdCl_2$, reagent, dissolved in 0.04 *M* aqueous NH_3/NH_4NO_3) over a basic ion-exchange column (Amberlite IRA-400, Rohm and Haas). The zeolite and metal solution were stirred for 12 h at a pH maintained slightly above 10.5. The slurry was filtered, and the zeolite dried at 400 K. Analysis of pre- and postexchange solutions was by atomic absorption on a Varian Model 1475 spectrophotometer. The Pd content of the zeolite was confirmed by oxidizing the Pd at 1400 K, dissolving the oxidized metal in concentrated HNO_3 according to published procedures (*16*), and analyzing the filtrate by AA.

Catalyst Characterization

Transmission spectra of the zeolites were obtained using an IBM IR/32 FTIR spectrometer at 4 cm^{-1} resolution. The zeolites

were pressed into wafers and dried at 10^{-4} Pa and 573 K for 4 h. Helium (Matheson, 99.999%, further purified by passage through 4A molecular sieve) at 573 K was flowed over the wafers for 1 h to reduce the Pd to metal according to the procedure of Reagan *et al.* (*17*). Spectra were recorded in a helium atmosphere at 573 and 298 K.

Powder X-ray diffraction patterns were obtained using a Phillips APD 3720 diffractometer with Cu$K\alpha$ radiation. The scan range was 2.0–70.0° (2θ) at 0.04°/s. The patterns were recorded under ambient conditions, but the zeolites were calcined in helium at 573 K for 4 h prior to analysis in order to reduce the palladium.

Scanning electron micrographs of some of the zeolites were taken at Exxon Research and Development Labs, Baton Rouge, at 20 kV accelerating voltage. Prior to analysis, the samples were mounted with epoxy and gold-sputtered.

Surface areas of the zeolites were estimated by BET analysis. The adsorption of 2-methylpentane (Phillips, research grade) at 303 K from a decalin (Phillips, research grade) solution was also measured. The solid and liquid were contacted for 24 h in a shaker bath, and then the composition of the equilibrium liquid was measured by GC (Gow-Mac Model 750P with an FID). The components were separated using a 1.8-m-long, 0.318-cm-o.d., 3% SE30 on Chromasorb W column at 353 K.

The isomerization experiments were conducted using a conventional horizontal tubular microreactor. The zeolites were calcined in flowing helium at 573 K for 4 h prior to the experiment. The reactor was stainless steel, 15 cm long, 1.27 cm o.d., and was located in a thermostated oven which maintained the reactor temperature ±1 K from the setpoint. About 1 g of catalyst was placed between plugs of silanized glass wool surrounded by 20/40-mesh glass beads on either end.

The hydrocarbon feed to the reactor was 2.0 ± 0.1% (volume) isobutene (Matheson, 99%, major impurities the other butene isomers) in *n*-butane (Matheson, 99%, major impurities isobutane and propane). The feed was prepared by liquefying the butene and then adding the proper volume by syringe injection to a sample cylinder of butane, fitted with a septum, at known pressure. The combined feed stream to the reactor was 10 vol% hydrocarbons and 90% of either (a) N_2 (Liquid Carbonic, 99.9%) or (b) 10% H_2/90% N_2 (Matheson, Certified Standard), both purified by passage through 4A molecular sieve. The total feed flow rate was 40 cc/min. The individual stream flow rates were controlled by Brooks Model 8744 manual flow controllers accurate to 0.5 cc/min.

The products were separated in the Gow-Mac GC using a 1.8-m-long, 0.318-cm-o.d., 0.3% Carbowax 20M on 80/100-mesh Carbopack C (Alltech) column, temperature programmed with a 3-min delay at 303 K, a 15 K/min ramp to 398 K, and then a 2-min hold. The products were first identified by relative retention. These identifications were confirmed by GC/MS, using a Finnigan 1020 MS in the electron-impact mode at 70 eV.

RESULTS

Catalyst Characterization

The results of chemical microanalyses for fluoride and palladium content (Galbraith Labs, Knoxville) are given in Table 1. The percentage replacement of –OH groups ("nominal replacement") was estimated by assuming a one-for-one replacement of –OH with F^-.

The XRD patterns for H-mordenite and some of its fluorided modifications are given in Fig. 1. The diffraction pattern for Pd-mordenite (sample A0) was the same as that for H-mordenite (sample B0). The five most intense peaks, corresponding to reflections (*18*) 202, 150, 200, 060, and 330 (*hkl*), were used to compute the unit cell constants of the zeolites. These remained essentially unchanged even after fluoridation: a = 18.0 A; b = 20.2 A; c = 7.5 A.

TABLE 1

Zeolite Microanalysis

Zeolite designation	Wt% F	Wt% Pd	% OH replacement
A0	0.0	1.0	0.0
A1	0.277	1.2	8.3
A2	0.396	1.1	12.1
A3	0.91	1.1	27.6
A4	6.67	1.3	100.0
B0	0.0	0.0	0.0
B1	0.28	0.0	8.3
B2	0.40	0.0	12.1
B3	0.92	0.0	27.6
B4	6.75	0.0	100.0

The scanning electron micrographs of powdery crystals of H-mordenite (sample B0) and a fluorided Pd-mordenite (A4) are shown in Fig. 2. Although the distribution of particle sizes is considerable, it is notable that there are no gross differences in average crystal size (on the order of 0.5–1 μm) or in the size distribution between the two zeolites. However, the micrograph for A4 differs from all the others in that for this sample the crystals appear less well defined.

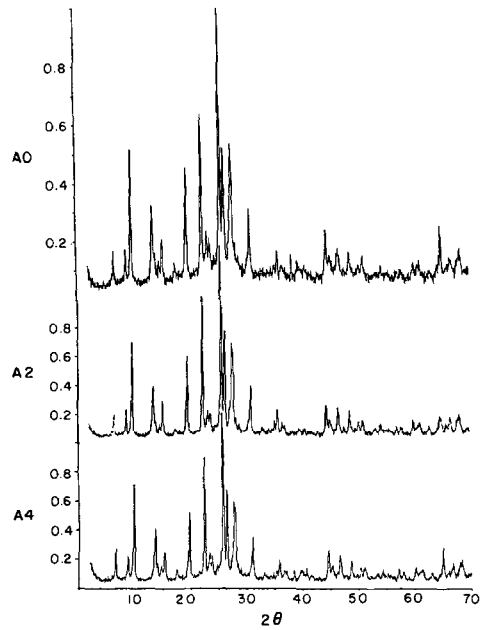

FIG. 1. X-ray diffraction patterns of unfluorided (A0) and fluorided (A2, A4) Pd-mordenites.

The BET surface areas and the moles of adsorbed 2-methylpentane per weight of zeolite are plotted in Fig. 3 as a function of the nominal percentage replacement of –OH groups.

The IR spectra of the zeolites were the same at the two temperatures examined; typical spectra are given in Fig. 4. There are at least two observable O–H stretching bands in H-mordenite, the primary one at 3610–3640 cm^{-1} and a shoulder at ca. 3740 cm^{-1} (*4*, *16*, *19*). The primary band is attributed to crystalline –OH groups and also –OH groups formed by dealumination. The shoulder is attributed to the O–H vibration in amorphous impurities or in silanol groups on the external surfaces of crystals. The spectra in Fig. 4 show that these bands as well as a broad band characteristic of adsorbed water centered at ca. 3260 cm^{-1} are present. The spectra of the fluorided modifications of these zeolites were qualitatively similar. The O–H group frequencies of the unfluorided and fluorided Pd-mordenites are given in Table 2. There is a relationship between the primary –OH band and the nominal percentage

TABLE 2

Band Frequencies in the Hydroxyl Region for Pd-Mordenites

Zeolite designation	Frequency (cm^{-1})	Assignment
A0	3723	Silanol
	3644	Crystalline
	3265	Bound H_2O
A1	3720	Silanol
	3638	Crystalline
	3265	Bound H_2O
A2	3636	Crystalline
	3269	Bound H_2O
A3	3622	Crystalline
	3258	Bound H_2O
A4	3595	Crystalline
	3260	Bound H_2O

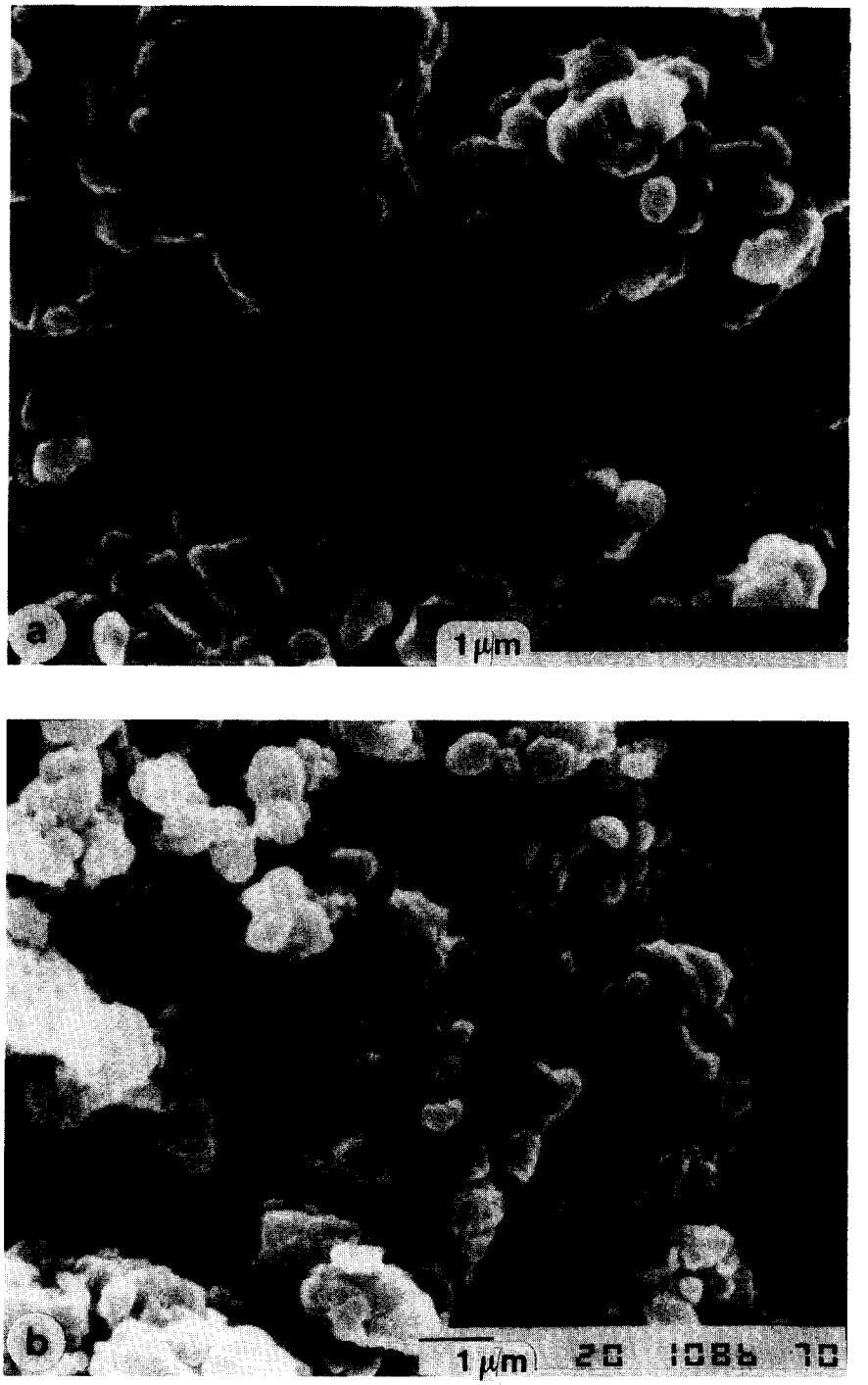

FIG. 2. Scanning electron micrographs of zeolite powders at 10,000× magnification: (a) H-mordenite (B0); (b) fluorided mordenite, >100% nominal replacement of –OH groups (A4).

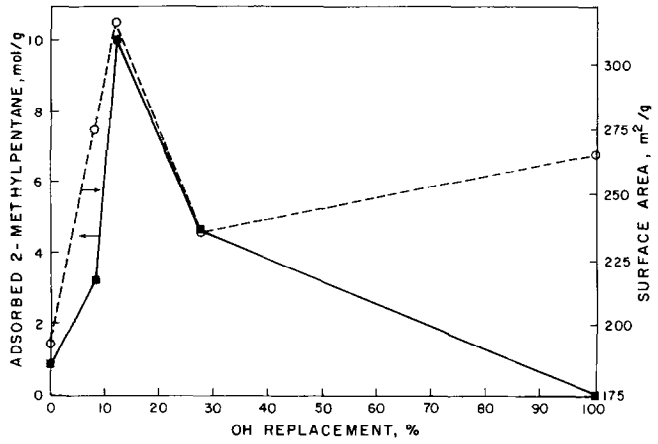

FIG. 3. BET surface areas (solid line) and 2-methylpentane adsorption capacities (from decalin solution at 303 K, dashed line) for Pd-mordenites.

replacement of –OH groups which is readily apparent upon plotting the frequency and apparent integrated intensity (AII) of this band as shown in Fig. 5.

Reactions of n-Butane/Isobutene (C_4)

The major products of the reactions were isobutane, ethane, propane, and the pentane isomers. Trace amounts of other hydrocarbons such as methane, ethylene, propylene, and the hexane isomers were also observed. It was possible to limit the conversion of *n*-butane in most cases to <15%. Turnover frequencies were calculated using

$$N = (XvC_b)/W \quad (1)$$

where N is the turnover frequency in mol/g·s, v the volumetric flow rate of the feed, C_b the C_4 concentration in the feed, and W the catalyst weight. The fractional conversion X was computed from the observed product amounts,

$$X = \Sigma_i[(F_i)_{out} - (F_i)_{in}](C \text{ number})_i/4, \quad (2)$$

where F_i is the molar flow rate of product i. The space-time yields to the products are the individual terms in the summation of Eq. (2). Selectivities were computed as (mol i/total mol products) × 100.

The stability of an unfluorided zeolite (A0) was examined with and without H_2 in the feed, as shown in Fig. 6. The deactivation behavior of the fluorided Pd-mordenites A1–A3 was qualitatively similar to that of A0. The heavily fluorided A4 (100% nominal –OH replacement) was inactive at all temperatures studied.

The effect of the isobutene was explored by performing one experiment with an olefin-free feed; the results of this and a comparable experiment with isobutene included in the feed are given in Fig. 7. The detailed product distributions from the C_4 reactions catalyzed by unfluorided and fluorided Pd-mordenites and H-mordenite are given in

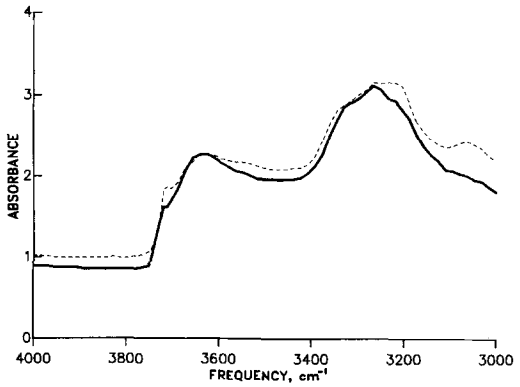

FIG. 4. IR spectra of H-mordenite (B0, dashed line) and Pd-mordenite (A0, solid line) in helium atmosphere at 573 K.

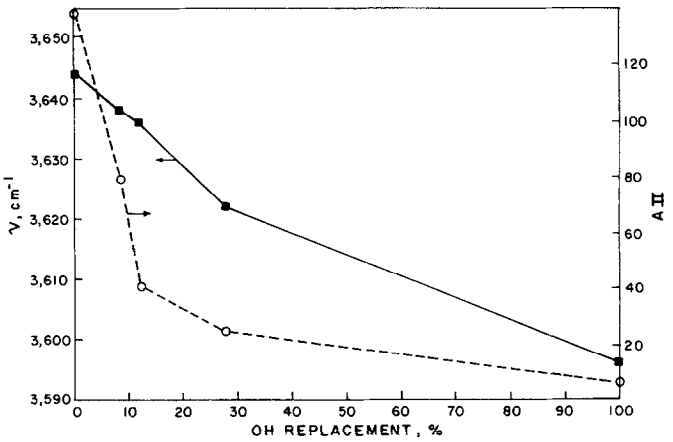

FIG. 5. Frequency (ν) and apparent integrated intensity (AII) of the crystalline O–H band in Pd-mordenites.

Table 3, while the total turnover frequencies to the major products of carbon numbers 2–5 are plotted at temperatures of 533, 553, and 573 K in Fig. 8. The turnover frequencies for H-mordenite (B0) are omitted for the sake of clarity, because at zero time on stream they are similar to the results for A0.

DISCUSSION

Structure of Fluorided Mordenites

The "A" series of Pd-mordenites all contained about 1.1 wt% Pd when dry (Table 1). This composition corresponds to replacement of ~1/16 of the exchangeable ions or one metal ion per two unit cells. From Table 1 it is also seen that the fluorine contents of samples A1–A3 exceeded the target values in the synthesis (5, 10, and 20% –OH replacement), indicating a high exchange efficiency. For sample A4, the fluorine content corresponds to >100% –OH group replacement; therefore, for this zeolite F^- must also have been used for purposes other than –OH replacement.

The diffraction pattern for Pd-mordenite (A0) was essentially the same as that for

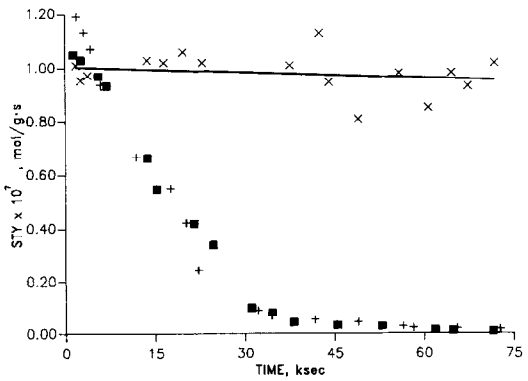

FIG. 6. Isobutane formation (space-time yield) in C_4 conversion at 573 K: ×, Pd-mordenite (A0) with 9 vol% H_2 included in feed; ■, A0 with no H_2 in feed; +, H-mordenite (B0) with 9 vol% H_2 in feed.

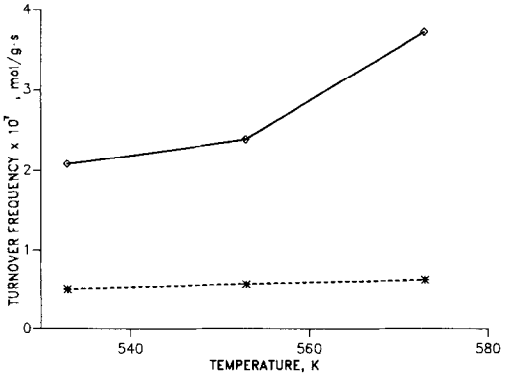

FIG. 7. Total product formation in C_4 conversion catalyzed by fluorided Pd-mordenite A2: solid line, with 0.2 vol% isobutene in hydrocarbon feed; dashed line, no isobutene in feed.

TABLE 3

Selectivities in C_4 Reactions

Zeolite designation	Temperature (K)	Selectivity to			
		Ethane	Propane	Isobutane	Pentanes
B0	533	14.2	26.3	59.3	0.2
	553	13.6	25.2	56.2	5.0
	573	21.3	28.9	40.1	9.7
A0	533	12.4	32.9	54.4	0.3
	553	13.6	27.9	50.3	8.2
	573	25.3	30.7	31.4	12.6
A1	533	6.1	13.7	79.0	1.2
	553	7.8	17.8	59.9	14.5
	573	11.0	17.5	27.4	44.1
A2[a]	533	11.8	33.9	54.3	0.0
	553	8.4	33.6	58.0	0.0
	573	13.3	31.4	55.3	0.0
A2	533	0.6	7.5	71.0	20.9
	553	0.4	10.2	49.0	40.4
	573	0.4	11.7	38.1	49.8
A3	533	0.0	14.5	33.6	51.9
	553	0.0	9.3	69.9	20.8
	573	0.0	11.7	69.7	18.6

[a] No isobutene in the hydrocarbon feed.

H-mordenite (B0). In a study of $PdNaNH_4$–Y zeolites, Bergeret *et al.* (*20*) found that the absence of extra peaks (uncharacteristic of Na–Y) at $2\theta = 20 \pm 5°$ indicates that the Pd in zeolites is atomically dispersed. The diffraction patterns of Fig. 1 show no low-intensity peaks at $2\theta = 20 \pm 5°$. All the observed peaks in this region correspond to peaks of H-mordenite. Since even the most intense peak in the region, at 19.75°, is only 0.2° wide at half-height, it is unlikely that peaks characteristic of the metal are obscured. Further evidence for a high dispersion of metal is found on comparing the different BET surface areas of samples B0 (260 ± 40 m^2/g) and A0 (190 ± 40 m^2/g). Clustered Pd in occlusions between zeolite crystals would be expected to have a negligible effect on the BET surface area.

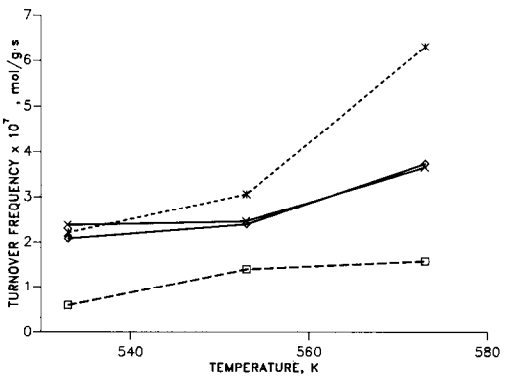

FIG. 8. Total product formation in C_4 conversion catalyzed by Pd-mordenites: —×—, sample A0; --*--, A1; —◇—, A2; --□--, A3.

Treatment with F^- does not alter the diffraction pattern of Pd-mordenite (Fig. 1) except in the case of sample A4. For A4 the low-angle peaks, those at $2\theta < 25°$, are shifted to higher 2θ by 0.01–0.05°. For $2\theta > 25°$, the peaks are shifted higher by 0.08–0.15°. The shift to higher angles is an indication of dealumination of the crystals (*21*, *22*), as are the increased (by about 20%)

intensities of the low-angle peaks (*3*). Dealumination is not surprising given the severe nature of the fluoride treatment for sample A4. The formation of a separate AlF_3 phase is one likely consequence of this dealumination; the reaction of Al_2O_3 with NH_4F is rapid under the synthesis conditions (*23*). The formation of AlF_3 would also account for the high level of fluorine incorporation in A4. Partial destruction of crystallinity associated with dealumination could also be responsible for the slight differences between the micrographs of samples B0 and A4 (Fig. 2).

The progressive fluoridation of the zeolite crystals by –OH replacement can be postulated on the basis of consideration of the adsorption and IR spectroscopic data. The adsorption capacities of zeolites A0–A3 for both N_2 and 2-methylpentane are quite similar, as seen from Fig. 3. The increase in adsorption capacity for nonpolar adsorbates with fluorine content suggests increasing adsorbent hydrophobicity. These higher adsorbate capacities were accompanied by decreases in the AII of the O–H band for bound water in the IR spectrum (at ~3260 cm^{-1}, Fig. 4), also indicative of increasing adsorbent hydrophobicity. The slightly reduced surface area of A3 probably results from crystal disruption or pore blockage accompanying slight dealumination; a similar phenomenon has been observed for acid-leached mordenites (*5, 24*).

As expected for the progressive replacement of –OH groups with F^-, the AII of the crystalline O–H stretching vibration is reduced, ultimately to less than 10% of the original AII (for sample A0) in the case of sample A4 (Table 2 and Fig. 5). As the number of Brønsted sites is reduced, the crystalline O–H stretching frequency decreases, suggesting an increase in acid strength for fluorided mordenites (*4, 5*); this behavior has been ascribed to the greater inductive effect of the F atoms adjacent to the remaining –OH groups.

With increasing fluoridation, the IR band at ~3720 cm^{-1} also decreases in frequency and eventually disappears. Because fluoridation likely proceeds from external crystal surfaces inward, this result suggests that the band at ~3720 cm^{-1} should be attributed to silanol groups on external surfaces rather than amorphous impurities. This result is also consistent with the hypothesis that acid sites are removed primarily by framework –OH replacement, rather than by dealumination, in samples A1–A3. In acid-leached, dealuminated mordenites, the AII of this band actually increases (*25*).

Kinetics of the C_4 Reactions

The turnover frequencies given in Fig. 8 indicate kinetic rather than diffusional control of the reactions; the Weisz–Prater modulus (*26*), assuming a first-order reaction, was calculated as 8×10^{-3} for catalyst A0 operating at 573 K. The modulus Φ is given by

$$\Phi = \frac{(N\rho_c)(L/2)^2}{D_e C_b}, \qquad (3)$$

where ρ_c is the crystalline density. The crystal characteristic length L was estimated from the SEM results as 1.0 μm, and a minimum effective diffusivity D_e of 1.0×10^{-7} cm^2/s was estimated from diffusivity data at lower temperatures (*27*). Using Fig. 6, it was calculated that zeolite A0 experienced 1.3 turnovers for isobutane formation over a 30-h period when 9.0 vol% H_2 was incorporated in the feed. Since other products were formed as well, the reaction can be characterized as catalytic.

Both Pd and H_2 were necessary to maintain catalytic activity, as Fig. 6 shows. The function of the Pd may have been to hydrogenate coke precursors, as does Pt in commercial dual-function isomerization catalysts. For catalysts A0 and B0, the equivalence in the product distributions and turnover frequencies observed at zero time on stream demonstrates that the Pd did not participate in the primary reactions of *n*-butane. Hypothesizing the absence of a bifunctional hydroisomerization mecha-

nism for the primary reactions is in accord with the findings of Ribeiro *et al.* (*28*), who found that for zeolites with strong acid sites the metal's sole function is to hydrogenate naphthenic coke precursors. The fact that reduced Pt and Ni do affect the primary reactions when the catalysts are metal-containing Y zeolites of moderate acid strengths (*28–30*), at temperatures similar to those of this study, further indicates that the fluorided mordenites are strongly acidic. When the dispersed metal in the zeolite is the active component, the primary reaction of a normal paraffin is direct hydrocracking to methane, ethane, etc. (*28–31*), which was not the case here.

It is shown in Fig. 7 that the isobutane present in the feed accelerated the global reaction rate by roughly a factor of 5, an anticipated effect of olefin addition to paraffin feeds (*32–35*). This is also an indication that the isomerization may have occurred in part by a "classical" mechanism (*9, 10*),

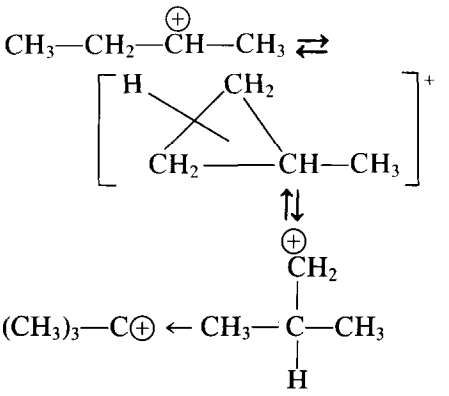

Although this mechanism has been postulated even for catalysis by zeolites, others (*10, 33, 36, 37*) have observed that, for certain strong acid catalysts, the reactions of normal paraffins can sometimes be explained in terms of several disproportionations in parallel. For *n*-butane, the most common disproportionation would be

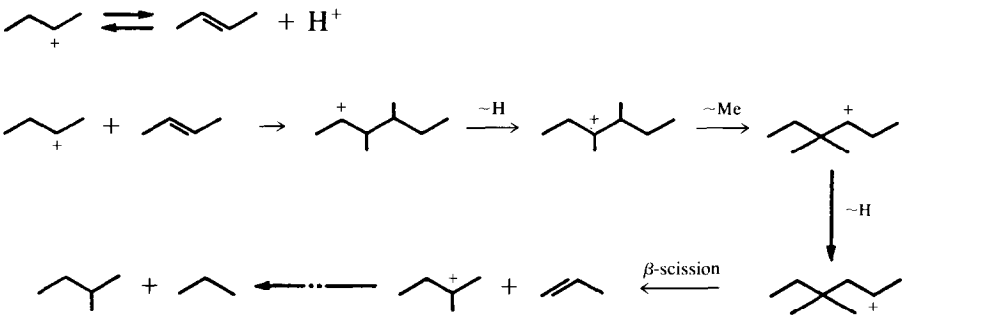

with subsequent alkylation-cracking reactions leading to isobutane, ethylene, etc. It is argued that the classical mechanism is unlikely because the intramolecular rearrangement must proceed through a high-energy primary carbenium ion, while the disproportionation route involves more stable intermediates.

The present data support the hypothesis that disproportionations are responsible for some of the observed products, because, while no pentanes or higher-molecular-weight products were formed when isobutene was excluded from the feed, the pentanes constituted a significant fraction of the products otherwise (Table 3, zeolite A2). Further evidence for disproportionation reactions is found in the lack of temperature dependence for the space-time yield of isobutane formation; the observed increases in turnover frequencies to C_2–C_5 products with respect to temperature (Fig. 8) generally result from increased STYs for the pentanes, ethane, and propane. However, the heavily fluorided A3 does not exactly follow this trend; although it catalyzes production of pentanes in high yield, the selectivity to pentanes decreases with

temperature. Nevertheless, for all the fluorided catalysts it can be concluded that the pentanes and isobutane are the dominant products. Considering that some of this isobutane was formed directly from the isobutene in the feed [2,2,4-trimethylpentane and the corresponding olefins are essentially the only products of isobutene hydrooligomerization at low conversion (*38, 39*), and these are cracked to give isobutane], it appears as if disproportionation rather than isomerization is the primary reaction of *n*-butane catalyzed by the fluorided mordenites.

It is interesting to compare the product distributions of the unfluorided catalysts (A0 and B0) to those of the fluorided catalysts A1–A3. For the former, ethane and propane constitute a significantly higher fraction of the products; in fact, these distributions are somewhat similar to that obtained using zeolite A2 in the absence of isobutene, and these results suggest the occurrence of protolytic cracking associated with strong acidity. For the fluorided catalysts, however, the selectivities to pentanes are higher, to ethane and propane lower. The paucity of light hydrocarbons can be explained if these fluorided zeolites catalyze secondary alkylation reactions consuming propylene and ethylene. The slightly anomalous behavior of catalyst A3 may be a consequence of partial dealumination and loss of crystallinity in this catalyst (note the loss of surface area in Fig. 3) or may simply be caused by a reduction in the number of Brønsted sites below a threshold at which contiguous adsorption of two hydrocarbons, which is necessary in both disproportionation and alkylation mechanisms, occurs readily.

The catalytic behavior of the fluorided vs unfluorided mordenites may be summed up by consideration of Fig. 9, which gives the ratio of the space-time yields of pentanes to propane as a function of temperature. Zeolites A1–A3 display ratios typically greater than one, while the unfluorided catalysts display ratios much less than one. A ratio of

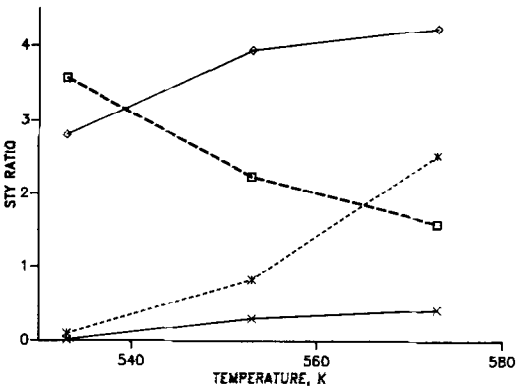

FIG. 9. Ratio of pentanes to propane space-time yields in C_4 conversion: —×—, sample A0; --*--, A1; —◇—, A2; --□--, A3.

one implies disproportionation in the absence of secondary reactions. Ratios less than one suggest that pentanes formed in the disproportionation reaction crack to lower hydrocarbons or that *n*-butane is cracked directly by a protolytic mechanism (*10–14*). This ratio being greater than one demonstrates that the fluorided mordenites are active for secondary alkylation reactions as well as for disproportionation. The optimum fluorine content for higher product formation appears to be about 12% nominal replacement of –OH groups, or 0.4 wt% in this case.

The alkylation activity of the fluorided mordenites may result from enhanced hydrophobicities as reflected by higher adsorption capacities for N_2 and 2-methylpentane (Fig. 3), the bimolecular surface reaction of two adsorbed hydrocarbons being considered necessary for alkylation. In contrast, although the classical isomerization mechanism includes a bimolecular hydride transfer step, this step is typically not rate-limiting for the isomerization of *n*-butane (*9–11*).

CONCLUSION

The mildly fluorided Pd-mordenties A1 and A2 are structurally quite similar to the parent Pd-mordenite, the main difference being partial replacement of –OH groups by

fluoride. These modifications can also be more active for acid catalysis of reactions of normal light paraffins (Fig. 7) than the comparable unfluorided zeolites. The enhanced acid strengths of fluorided mordenites, as suggested by the IR data given here and by pyridine TPD measurements elsewhere (*5*), probably contribute to the greater activity. Far more important than higher activities, however, are the enhanced selectivities of the mildly fluorided mordenites for the formation of the pentane isomers by disproportionation, possibly followed by secondary alkylation reactions. The prevalence of such reactions, all of which involve two adsorbed hydrocarbons, may be related to the higher capacities of these zeolites for nonpolar adsorbates. It is evident that these or similar catalyst formulations may prove useful in the alkylation reactions of light hydrocarbons.

ACKNOWLEDGMENTS

The authors thank Dr. Ray Ferrell, Jr., Mr. X. B. Cox, and Mr. James Clark for their assistance in the experimental work. James Maness was the recipient of a fellowship provided by the Exxon Foundation.

REFERENCES

1. Choudhary, V. R., *Ind. Eng. Chem. Prod. Res. Dev.* **16,** 12 (1977).
2. Ghosh, A. K., and Kydd, R. A., *Catal. Rev. Sci. Eng.* **27,** 539 (1985).
3. Lok, B. M., Gortzema, F. P., Messina, C. A., Rastell, H., and Izod, T. P. J., *in* "Intrazeolite Chemistry" (F. G. Dwyer and G. D. Stucky, Eds.), ACS Symp. Ser., Vol. 218, p. 41. Amer. Chem. Soc., Washington, DC, 1983.
4. Becker, K. A., and Kowalak, S., *J. Chem. Soc. Faraday Trans. 1* **81,** 1161 (1985).
5. Ghosh, A. K., and Kydd, R. A., *J. Catal.* **103,** 399 (1987).
6. Auroux, A., Bolis, V., Wierzchowski, P., Gravelle, P. C., and Vedrine, J. C., *J. Chem. Soc. Faraday Trans. 1* **75,** 2544 (1979).
7. Taniguchi, H., Masuda, T., Tsutsumi, K., and Takahashi, H., *Bull. Chem. Soc. Japan* **53,** 2643 (1980).
8. Schlup, J. R., and Vaughan, R. W., *J Catal.* **99,** 304 (1986).
9. Brouwer, D. M., and Hogeveen, H., *in* "Progress in Physical Organic Chemistry" (A. Streitwieser, Jr., and R. W. Taft, Eds.), Vol. 9, p. 179. Wiley, New York, 1972.
10. Fajula, F., *in* "Catalysis by Acids and Bases" (B. Imelik, C. Naccache, Y. Ben Taarit, and J. C. Vedrine, Eds.), p. 361. Elsevier, Amsterdam, 1985.
11. Olah, G. A., *Angew. Chem. Int. Ed. Engl.* **12,** 173 (1973).
12. Haag, W. O., and Dessau, R. M., "Proceedings, 8th International Congress on Catalysis, Berlin, 1984," p. 305. Verlag-Chemie, Weinheim, 1984.
13. Olah, G. A., Halpern, J., Shen, J., and Mo, Y. K., *J. Amer. Chem. Soc.* **95,** 4960 (1973).
14. Larsen, J. W., *J. Amer. Chem. Soc.* **99,** 4379 (1977).
15. Dooley, K. M., and Gates, B. C., *J. Catal.* **96,** 347 (1985).
16. Weeks, T. J., Hillery, H. F., and Bolton, A. P., *J. Chem. Soc. Faraday Trans. 1* **72,** 2051 (1976).
17. Reagan, W. J., Chester, A. W., and Kerr, G. T., *J. Catal.* **69,** 89 (1981).
18. Meier, W. M., and Olson, D. H., "Atlas of Zeolite Structure Types." Structure Commission of the Intl. Zeolite Assn., 1978.
19. Karge, H. G., *Z. Phys. Chem. (Wiesbaden)* **95,** 241 (1975).
20. Bergeret, G., Gallezot, P., and Imelik, B., *J. Phys. Chem.* **85,** 411 (1981).
21. Eberly, P. E., Jr., and Kimberlin, C. N., Jr., *Ind. Eng. Chem. Prod. Res. Dev.* **9,** 335 (1970).
22. Olsson, R. W., and Rollmann, L. D., *Inorg. Chem.* **16,** 651 (1977).
23. Aneke, L. E., Gerritsen, L. A., van den Berg, P. J., and de Jong, W. A., *J. Catal.* **59,** 26 (1979).
24. Hopper, J. R., and Voorhies, A., Jr., *Ind. Eng. Chem. Prod. Res. Dev.* **11,** 294 (1972).
25. Kredel, P., and Fetting, F., "Proceedings, 8th International Congress on Catalysis, Berlin, 1984," p. 569. Verlag-Chemie, Weinheim, 1984.
26. Froment, G. F., and Bischoff, K. B., "Chemical Reactor Analysis and Design," Chap. 3. Wiley, New York, 1979.
27. Paravar, A., and Hayhurst, D. T., "Proceedings, 6th International Zeolite Conference, Reno, 1983," p. 217. Butterworths, Guildford, UK, 1984.
28. Ribeiro, F., Marcilly, C., and Guisnet, M., *J. Catal.* **78,** 275 (1982).
29. Tri, P. L., Messardier, J., Gallezot, P., and Imelik, B., *J. Catal.* **85,** 244 (1984).
30. Law, P. L., and Kenney, C. N., *J. Catal.* **64,** 241 (1980).
31. Gray, J. A., and Cobb, J. T., Jr., *J. Catal.* **36,** 125 (1975).
32. Pines, H., and Wackher, R. C., *J. Amer. Chem. Soc.* **68,** 595, 599 (1946).
33. Condon, F. E., *in* "Catalysis" (P. H. Emmett, Ed.), Vol. 6, Chap. 2. Reinhold, New York, 1958.

34. McCaulay, D. A., *J. Amer. Chem. Soc.* **81,** 6437 (1959).
35. Kramer, G. M., Skomorowski, R. M., and Hinlicky, J. A., *J. Org. Chem.* **28,** 2085 (1963).
36. Fuentes, G. A., and Gates, B. C., *J. Catal.* **76,** 440 (1982).
37. Bearez, C., Chevalier, F., and Guisnet, M., *React. Kinet. Catal. Lett.* **22,** 405 (1983).
38. Lapidus, A. L., Isakov, Ya. I., Rudakova, L. N., Minachev, Kh. M., and Eidus, Ya. T., *in* "Proceedings of the Symposium on the Mechanisms of Hydrocarbon Reactions" (F. Marta and D. Kallo, Eds.), p. 403. Elsevier, New York, 1973.
39. Onopchenko, A., Cupples, B. L., and Kresge, A. N., *Ind. Eng. Chem. Prod. Res. Dev.* **22,** 182 (1983).